Title

Quantification of Analyte Concentration in the Single Molecule Regime Using Convolutional Neural Networks

Journal

Analytical Chemistry, 91(21)

ISSN

0003-2700

Authors

Thrift, William John

Ragan, Regina

Publication Date

2019-11-05

DOI

10.1021/acs.analchem.9b03599

analytical chemistry

Letter

Cite This: *Anal. Chem.* 2019, 91, 13337−13342

pubs.acs.org/ac

Quantification of Analyte Concentration in the Single Molecule Regime Using Convolutional Neural Networks

William John Thrift and Regina Ragan*

Department of Materials Science and Engineering, University of California, Irvine, Irvine, California 92697-2585, United States

Supporting Information

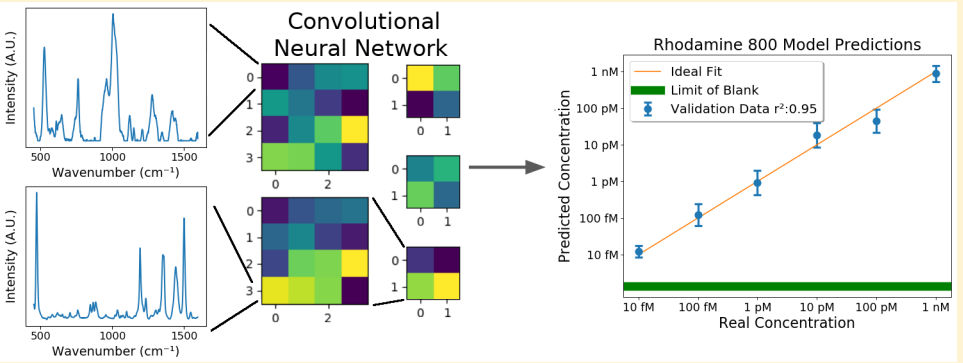

ABSTRACT: Single molecule (SM) detection represents the ultimate limit of chemical detection. Over the years, many experimental techniques have emerged with this capacity. Yet, SM detection and imaging methods produce large spectral data sets that benefit from chemometric methods. In particular, surface enhanced Raman scattering spectroscopy (SERS), with extensive applications in biosensing, is demonstrated to be particularly promising because Raman active molecules can be identified without recognition elements and is capable of SM detection. Yet quantification at ultralow analyte concentrations requiring detection of SM events remains an ongoing challenge, with the few existing methods requiring carefully developed calibration curves that must be redeveloped for each analyte molecule. In this work, we demonstrate that a convolutional neural network (CNN) model when applied to bundles of SERS spectra yields a robust, facile method for concentration quantification down to 10 fM using SM detection events. We further demonstrate that transfer learning, the process of reusing the weights of a trained CNN model, greatly reduces the amount of data required to train CNN models on new analyte molecules. These results point the way for unambiguous analysis of large spectral data sets and the use of SERS in important ultra low concentration chemical detection applications such as metabolomic profiling, water quality evaluation, and fundamental research.

Optical detection and spectroscopy of single molecules in the condensed phase has uncovered a wealth of understanding of molecular dynamics in physical, chemical, and biological systems since the first measurement in 1989 using frequency modulated laser spectroscopy by Moerner and Kador.[1] Compared to other single molecule (SM) detection schemes, SM surface enhanced Raman scattering (SERS), first reported in 1997,[2,3] has several advantages, including the ability to directly sense nonemitters and nonresonant molecules with small Raman cross sections.[4−6] SERS acquires rich spectral information from the "fingerprint" region in vibrational spectroscopy which can be used to uniquely identify molecules,[7] enabling multiplexing.[8]

Like many fields within analytical chemistry, SERS spectroscopy has greatly benefited from the development of chemometric methods. Principal component analysis (PCA) dimensional reduction,[9] is now ubiquitous in SERS analysis, for example, being used for detecting cancer.[10−13] Linear[14−16] and multilinear[17,18] regressions are common for concentration quantification using the Langmuir adsorption curve.[19] The ongoing machine learning revolution has begun to impact SERS, including using support vector machines[20,21] and decision trees[22,23] to analyze spectra. Fully connected artificial neural networks have been used for quantification of concentration in the micromolar regime,[24] and convolutional neural networks (CNNs) have been used to differentiate metabolites produced by cells *in vitro*.[25] These machine learning techniques have greatly improved predictions because they are robust to noise and nonanalyte signal and can handle deviations from the Langmuir isotherm, but they map one spectrum to one concentration value. SM SERS is characterized by discrete jumps in analyte number observed in any given measurement, so concentration will not be correctly inferred from one measurement.[26] This observation has led to quantification methods based on mapping the distribution of analyte observations to concentration such as the Brulé methods[27] and the digital method.[28] However, these methods

Received: August 7, 2019
Accepted: October 7, 2019
Published: October 7, 2019

DOI: 10.1021/acs.analchem.9b03599
Anal. Chem. 2019, 91, 13337−13342

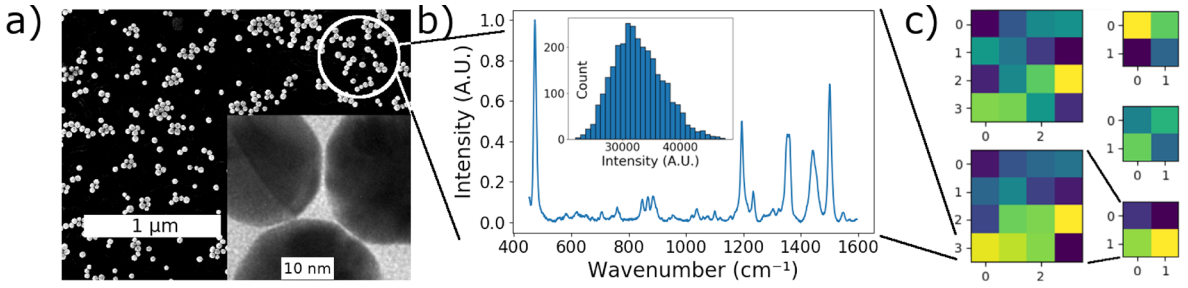

Figure 1. (a) SEM image of as-assembled gold nanoparticle assemblies. Inset depicts a TEM image of hotspots in an as-assembled gold nanoparticle assembly, and gap spacings are observed to be 0.9 nm. (b) Preprocessed SERS spectrum with an R800 concentration of 1 μM. Inset depicts the 1441 cm^{-1} vibrational mode signal distribution of a 1 μM R800 data set, an RSD of 13.1% is observed. (c) Schematic of a CNN mode. Refer to Figure S1 for a depiction of the CNN model and Figure S4 for an example of a complete input into the CNN model.

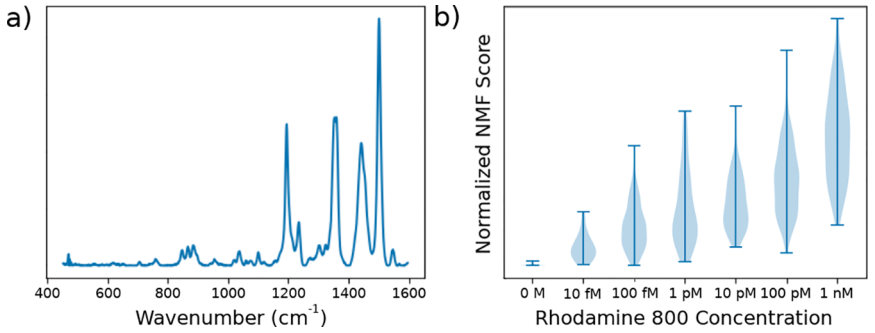

Figure 2. (a) NMF component of R800 acquired from 1 μM SERS measurements. (b) Violin plot of normalized NMF scores with respect to this component averaged from 64 spectra bins across the SM concentration regime. The top and bottom bars represent the maximum and minimum scores at each concentration, while the width of the distribution depict the density of spectra maps with those scores.

do not generalize to other analyte molecules, and entire data sets must be acquired for each new application, slowing their adoption in key applications such as measuring biomarkers[29,30] or contaminants in water.[31]

One of the most important applications of contemporary machine learning, i.e., image analysis, has remained relatively untouched by the SERS community. With newly developed SERS surfaces that have SERS enhancement factors of 10^9 and a relative standard deviation of 10% over large areas,[32] spectra are acquired across the SM concentration regime and are bundled into 8 × 8 pixel maps (with each pixel being a SERS spectra) and used to train a CNN model. The uniformity of enhancement factor is essential for our approach, as large variance in the data set not only increases the variance in predictions, which limits the methods to semiquantitative analysis[25] but also requires more data for convergence and prevents a transfer learning approach.[33] A key advantage of the proposed CNN analysis is its compatibility with transfer learning, the use of large data sets to train a model and then generalize this pretrained model to new molecules quickly with significantly smaller data sets. The presented CNN model is used to address the long-standing challenge in SERS: quantification of subnanomolar analyte concentrations. The demonstrated limit of blank (LOB) is 1 fM for Rhodamine 800, with a limit of quantification (LOQ) of 10 fM. Furthermore, the model's predicted concentrations have an average r^2 value of 0.958 over 6 orders of magnitude as determined by k-folds cross validation. Generalization of the CNN model to other analytes using transfer learning is demonstrated with methylene blue. Transfer learning achieves good results with as few as 50 8 × 8 pixel maps. Thus, entire data sets are acquired quickly, requiring just 5.3 min of total laser exposure time per concentration to train a robust model that is much faster and more scalable than required for building SM concentration regression models. This demonstrates a proof of concept for hyperspectral CNN image analysis of SERS, which could be broadly applicable within SERS, especially in the biological setting where classification of images could improve analysis of bacteria that are already imaged with SERS.[34−36]

RESULTS AND DISCUSSION

Experimental System. Integral to any machine learning approach are access to large and high-quality data sets. Using 2-dimensional physically activated chemical (2PAC) self-assembly, we have shown we can achieve reproducible enhancement factors of 10^9 over 1 cm^2.[32] 2PAC cross-links nanoparticles into discrete assemblies with a small molecule linker, where the cross-linking reaction is driven by electrohydrodynamic flow at on a substrate surface and is described in detail elsewhere.[32] A scanning electron microscopy (SEM) image of a 2PAC assembled SERS surface is depicted in Figure 1a. The inset of Figure 1a depicts a transmission electron microscopy (TEM) image of hotspots observed in a 2PAC fabricated assembly, the observed gap spacing is 0.9 nm, corresponding to the length of the chemical cross-linker.[32] Large area SERS maps are acquired from these 2PAC assembled surfaces, as described in the Experimental Details in the Supporting Information. Analyte dissolved in water is used as the immersion media for a water immersion objective during measurements. Spectra are preprocessed, which includes Savitsky−Golay smoothing and background subtraction as described in the Experimental Details in the Supporting Information. An example spectrum of Rhodamine

DOI: 10.1021/acs.analchem.9b03599
Anal. Chem. 2019, 91, 13337−13342

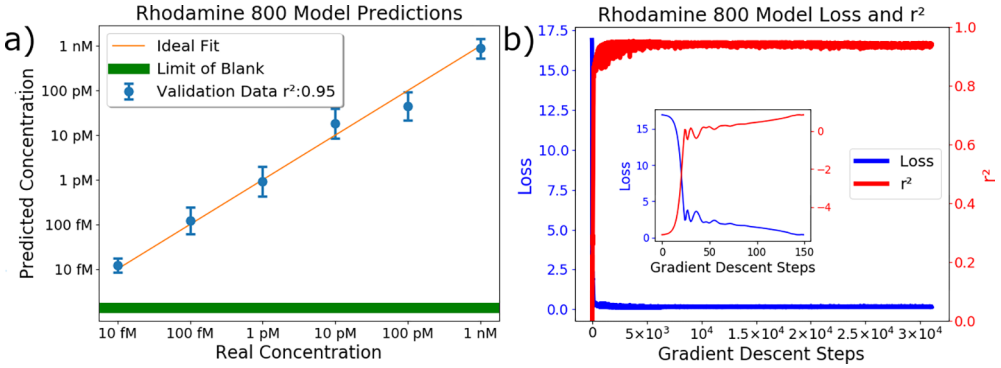

Figure 3. (a) Representative Rhodamine 800 concentration predicted by the CNN model on a test data set acquired during k-fold cross validation. (b) Model test loss and r^2 over gradient descent steps of the model depicted in Figure 3a. Inset: test loss and r^2 depicting local minima of loss when the model predicts similar concentrations for all inputs.

800 (R800) is depicted in Figure 1b, this spectrum was acquired at a concentration of 1 μM of R800. The inset of Figure 1b depicts the distribution of the R800 1441 cm^{-1} signal emerging across 2940 SERS spectra acquired at 1 μM concentration of R800. One may observe a relative standard deviation of 13.1%, and this is somewhat larger than the 10% reported previously[32] for chemisorbed benzenethiol, but the difference is unsurprising as R800 does not chemisorb onto gold and will thus exhibits a distribution of molecular location and orientation in the hotspot volume.

In order to analyze relevant spectral features in the high dimensional data, nonnegative matrix factorization (NMF) is used to identify and visualize features associated with R800 scattering events on sample surfaces. NMF is chosen over principal component analysis (PCA) because SERS spectra satisfy NMF's assumption of all positive signals, resulting in improved differentiation of spectral features that emerge from analyte and nonanalyte sources,[37] which is necessary in SM SERS where nonanalyte spectra will have more variation than analyte spectra. Each spectrum is reduced to 32 independent signals using NMF. Further details regarding the implementation of NMF are provided in the Supporting Information. An extracted NMF component vector associated with R800 is acquired only from a 1 μM R800 data set and depicted in Figure 2a. Here, in the many molecule detection regime, the SERS spectra is dominated by signal of vibrational modes from R800. This results in a NMF loading vector perfectly representing the R800 vibrational spectra with no contamination from nonanalyte signal being observed such as the Si peak from the substrate at 523 cm^{-1} in the experimental spectrum of Figure 1b. Thus, we use this extracted NMF loading vector to assess R800 score (the magnitude of the R800 associated component for a spectrum) of spectra acquired at trace concentrations (1 nM and below). Specifically, at these trace concentrations, we map bundles of 64 Raman spectra and test how accurately R800 score reflects analyte concentration. Groups of spectra are required since at trace concentrations many measurements may not have an analyte in the measurement area, thus concentration is determined by the presence of analyte signal exhibited in these spectral maps. We visualize the average R800 score of these 64 spectra groups as a function of concentration in Figure 2b. SERS spectra from each concentration considered here are depicted in Figure S2. The violin plots depict an upward trend of these average scores across the trace concentration regime. Yet factors such as the complex background arising from nonanalyte signals can cause a large variance in the R800 score. The nonlinear response of concentration as a function of the NMF score at concentrations below 1 nM is similar to those obtained by Albuquerque et al.[28] This complexity of providing a generalizable solution for accurately determining analyte concentration motivates a deep learning approach that is described below.

Convolutional Neural Network (CNN) for Single Molecule SERS Quantification. Our approach to determining the distribution of single molecule events in order to determine concentration begins with bundling SERS spectra into 8 × 8 pixel maps, where each pixel is a SERS spectrum, as depicted schematically in Figure 1c. It is important to bundle SERS spectra when the concentration is below 1 nM, i.e., some measurements in the laser spot size may not contain a molecule on the surface. These maps are randomly split into training (80%) and testing (20%) groups for k-fold cross validation. The SERS spectra is reduced to 32 independent signals using NMF that is trained using the training data set. An example of NMF scores obtained is depicted in Figure S4. During the training period, each map is given a log transformed concentration label. It is important to note that this is a different NMF trained than that obtained from the 1 μM data set; at concentrations below 1 nM molecular orientation,[38] vibronic coupling,[39] and other factors[40] will more heavily influence SERS spectra than at higher concentrations. The need for using multiple spectra when using SM detection events for quantification is further discussed in the Supporting Information.

The CNN architecture used in this work is depicted schematically in Figure S1. A relatively simple CNN model is used to avoid overfitting. A representative set of predictions from the CNN model trained on a test data set are shown in Figure 3a, where an r^2 of 0.95 over 6 orders of magnitude is determined. We perform a 5-fold cross validation to validate the model, observing a cross validation mean squared error (MSE) loss of 0.111 ± 0.029 and r^2 of 0.958 ± 0.012. The limit of blank (LOB) is determined to be 1.0 fM with a relative error of 1.1 fM/fM and the limit of quantification (LOQ) is approximately 10 fM. These results demonstrate that the CNN model is robust, producing good results without the need to fine-tune any parameters based on molecular adsorption models that was performed in prior methods. Figure 3b depicts the testing MSE loss as a function of gradient descent steps. One may observe the model briefly finding local minima

DOI: 10.1021/acs.analchem.9b03599
Anal. Chem. 2019, 91, 13337−13342

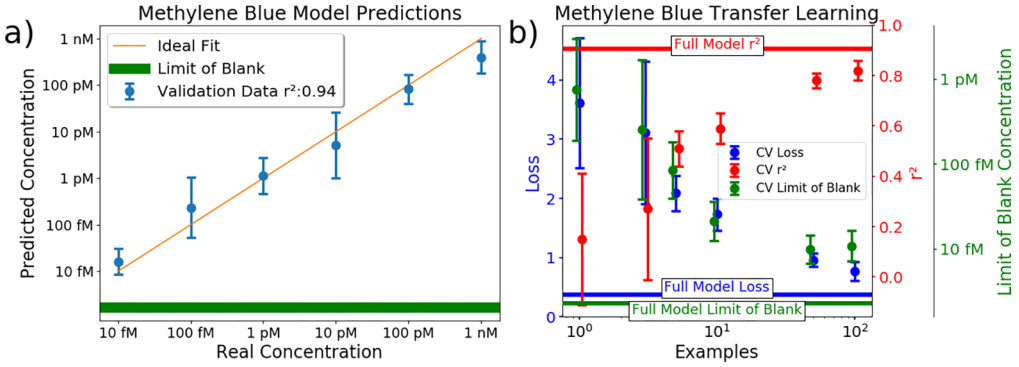

Figure 4. (a) Representative Methylene Blue concentration predicted by the CNN model on a test data set acquired during k-fold cross validation. (b) Cross validation loss, r^2, and LOB of transfer learned Methylene Blue model as a function of the number of unique input maps. The model is identical to that used in Figure 3 but with weights acquired from the Rhodamine 800 model depicted in Figure 3a, with the third and fourth convolutional layers frozen. Horizontal bars represent the metric performance depicted in Figure 4a. Number of examples for r^2 and LOB are offset by 5% for visual clarity.

corresponding to the degenerate solution of predicting all inputs as having identical concentrations, depicted in the inset of Figure 3b. The model then finds a good solution to the problem in just a few hundred gradient descent steps. Additionally, in order to ensure that the CNN model is not using Raman intensities related to unique features on a SERS substrate rather than the analyte, we have evaluated the performance of a R800 model applied to validation data acquired from a SERS substrate not used to train the CNN model. Similar prediction accuracy is observed in this case and results are provided in Figure S3.

Transfer Learning for New Analyte Molecule. Here, we demonstrate the generalizability of the R800 CNN model to another analyte, Methylene Blue (MB) using a transfer learning approach.[33] That is, pretrained weights from the R800 CNN model are used in the training of a MB CNN model in order to reduce the size of the training data needed for accurate predictions. The weights of the third and fourth convolutional layers are frozen throughout training. New NMF components are found using the MB training data set. The transfer learning process will fine-tune the unfrozen weights of the first and second convolutional layers, which have the important task of learning the pattern of the NMF scores that are associated with SM detection events of the new analyte. While these patterns are different from one molecule to the next, the pretrained CNN model weights will be much closer to final CNN weights for this new analyte than that of a randomly initialized CNN network and thus significantly reduce the amount of training data necessary. Similarly, different molecules will have different interaction strengths with the SERS surface (especially in the extreme case of chemisorption with, for example, thiolated molecules) and this will change the distribution of SM events expected at a particular concentration. Again, in this case, trained model weights on another analyte will still be much closer to the final weights of a model trained on a new analyte, making the transfer learning strategy data efficient.

First, we evaluate a MB CNN model trained from the full 56736 augmented MB training maps with the same architecture as the R800 CNN model. This provides a baseline for evaluating the performance of the transfer learning approach. The regression results are depicted in Figure 4a, where a cross validation MSE loss of 0.288 ± 0.085, r^2 of 0.932 ± 0.02, and LOB of 1.2 fM ± 1 fM are achieved. The loss, LOB and r^2 of this model, trained on a full MB data set, is used as the lower (upper) limit of transfer learned model performance depicted in Figure 4b as horizontal bars. We then test how much data is necessary to train a new model using transfer learning. We restrict the number of training examples, composed of an 8 × 8 bundle of SERS spectra, observed by the model to be between 1 and 100 per concentration, with each map being augmented 32-fold as described in the Supporting Information. One may observe near optimal model performance with as few as 50 training examples. Models trained without transfer learning from the R800 model with 100 or less examples are unable to escape the degenerate local minimum described previously. This effect also leads to large standard deviations in the cross validation values of metrics at 1 and 3 examples. Then, even at just 5 examples, the model is always able to escape the local minimum, resulting in much smaller variance of cross validation metrics. These results demonstrate that the R800 CNN model is broadly generalizable to SM concentration regressions. This is essential for most practical applications, for example, in metabolomics, where many different molecules may need to be validated to identify their importance in disease, or in water quality, where the background may vary significantly from place to place. With transfer learning, we no longer need to completely recreate our SM concentration quantification models.

CONCLUSION

In this work, a convolutional neural network (CNN) model is demonstrated to perform concentration regressions on bundles of SERS spectra composed of 8 × 8 pixel maps. This study shows that the CNN model dramatically simplifies the implementation of concentration regressions in the single molecule (SM) detection regime. Using Rhodamine 800 as the analyte, the CNN model makes excellent concentration predictions. Specifically, a 5-fold cross validated average r^2 of 0.958 is achieved with quantification down to 10 fM. Further, the model is generalizable to a different analyte (methylene blue) by the implementation of transfer learning. This strategy results in good predictions with as few as 50 training examples, which enables new data sets to be acquired in just 5.3 min per concentration. We believe that CNN models applied to maps of spectra can be generalized both to other SERS sensor platforms as well as other chemical analysis techniques capable

DOI: 10.1021/acs.analchem.9b03599
Anal. Chem. 2019, 91, 13337−13342

of single molecule detection. This will increase the pace of innovation in chemical sensing, enabling researchers to tackle long-standing problems like using rare, low concentration metabolites in building metabolomics models or in identifying ultralow concentration of toxins in waterlike microcystins.

■ ASSOCIATED CONTENT

Supporting Information

The Supporting Information is available free of charge on the ACS Publications website at DOI: 10.1021/acs.analchem.9b03599.

Experimental details: materials; 2PAC assembly; characterization; data analysis and models; convolutional neural network model; SERS spectra acquired with various concentrations of R800; CNN model predictions from SERS substrates not used in training the CNN model and a comparison with a commercially available SERS substrate; and graphical depiction of an example used in training the CNN model

■ AUTHOR INFORMATION

Corresponding Author

*E-mail: rragan@uci.edu.

ORCID

Regina Ragan: 0000-0002-8694-5683

Notes

The authors declare no competing financial interest.

■ ACKNOWLEDGMENTS

The authors acknowledge the National Science Foundation Grants EECS-1449397 and CBET-1926612 for funding this work. W.J.T. acknowledges support from the National Science Foundation BEST IGERT Program (Grant NSF DGE-1144901). The authors also acknowledge the use of the facilities within the Laser Spectroscopy Facility, and the Irvine Materials Research Institute at the University of California, Irvine.

■ REFERENCES

(1) Moerner, W. E.; Kador, L. *Phys. Rev. Lett.* **1989**, *62* (21), 2535−2538.

(2) Kneipp, K.; Wang, Y.; Kneipp, H.; Perelman, L. T.; Itzkan, I.; Dasari, R. R.; Feld, M. S. *Phys. Rev. Lett.* **1997**, *78* (9), 1667−1670.

(3) Nie, S.; Emory, S. R. *Science* **1997**, *275* (5303), 1102−1106.

(4) Blackie, E. J.; Le Ru, E. C.; Etchegoin, P. G. *J. Am. Chem. Soc.* **2009**, *131* (40), 14466−14472.

(5) Dieringer, J. A.; Wustholz, K. L.; Masiello, D. J.; Camden, J. P.; Kleinman, S. L.; Schatz, G. C.; Van Duyne, R. P. *J. Am. Chem. Soc.* **2009**, *131* (2), 849−854.

(6) Le Ru, E. C.; Grand, J.; Sow, I.; Somerville, W. R. C.; Etchegoin, P. G.; Treguer-Delapierre, M.; Charron, G.; Félidj, N.; Lévi, G.; Aubard, J. *Nano Lett.* **2011**, *11* (11), 5013−5019.

(7) Larkin, P. *Infrared and Raman Spectroscopy; Principles and Spectral Interpretation*; Elsevier, 2011.

(8) Kasera, S.; Herrmann, L. O.; Barrio, J. del; Baumberg, J. J.; Scherman, O. A. *Sci. Rep.* **2014**, *4*, 6785.

(9) Etchegoin, P. G.; Meyer, M.; Blackie, E.; Le Ru, E. C. *Anal. Chem.* **2007**, *79* (21), 8411−8415.

(10) Feng, S.; Chen, R.; Lin, J.; Pan, J.; Chen, G.; Li, Y.; Cheng, M.; Huang, Z.; Chen, J.; Zeng, H. *Biosens. Bioelectron.* **2010**, *25* (11), 2414−2419.

(11) Lin, D.; Feng, S.; Pan, J.; Chen, Y.; Lin, J.; Chen, G.; Xie, S.; Zeng, H.; Chen, R. *Opt. Express* **2011**, *19* (14), 13565−13577.

(12) Feng, S.; Chen, R.; Lin, J.; Pan, J.; Wu, Y.; Li, Y.; Chen, J.; Zeng, H. *Biosens. Bioelectron.* **2011**, *26* (7), 3167−3174.

(13) Feng, S.; Lin, D.; Lin, J.; Li, B.; Huang, Z.; Chen, G.; Zhang, W.; Wang, L.; Pan, J.; Chen, R.; et al. *Analyst* **2013**, *138* (14), 3967−3974.

(14) Lee, D.; Lee, S.; Seong, G. H.; Choo, J.; Lee, E. K.; Gweon, D.-G.; Lee, S. *Appl. Spectrosc.* **2006**, *60* (4), 373−377.

(15) Stevenson, R.; Ingram, A.; Leung, H.; C. McMillan, D.; Graham, D. *Analyst* **2009**, *134* (5), 842−844.

(16) Bodelón, G.; Montes-García, V.; López-Puente, V.; Hill, E. H.; Hamon, C.; Sanz-Ortiz, M. N.; Rodal-Cedeira, S.; Costas, C.; Celiksoy, S.; Pérez-Juste, I.; et al. *Nat. Mater.* **2016**, *15* (11), 1203−1211.

(17) Shafer-Peltier, K. E.; Haynes, C. L.; Glucksberg, M. R.; Van Duyne, R. P. *J. Am. Chem. Soc.* **2003**, *125* (2), 588−593.

(18) Nguyen, C. Q.; Thrift, W. J.; Bhattacharjee, A.; Ranjbar, S.; Gallagher, T.; Darvishzadeh-Varcheie, M.; Sanderson, R. N.; Capolino, F.; Whiteson, K.; Baldi, P.; et al. *ACS Appl. Mater. Interfaces* **2018**, *10* (15), 12364−12373.

(19) Langmuir, I. *J. Am. Chem. Soc.* **1918**, *40* (9), 1361−1403.

(20) Li, S.; Zhang, Y.; Xu, J.; Li, L.; Zeng, Q.; Lin, L.; Guo, Z.; Liu, Z.; Xiong, H.; Liu, S. *Appl. Phys. Lett.* **2014**, *105* (9), 091104.

(21) Dong, R.; Weng, S.; Yang, L.; Liu, J. *Anal. Chem.* **2015**, *87* (5), 2937−2944.

(22) Albuquerque, C. D. L.; Nogueira, R. B.; Poppi, R. J. *Microchem. J.* **2016**, *128*, 95−101.

(23) Huang, C.; Tsai, T.; Wen, B.; Chung, C.; Li, Y.; Chuang, Y.; Lin, W.; Li, L.; Wang, J.; Wang, Y.; et al. Hybrid SVM/CART Classification of Pathogenic Species of Bacterial Meningitis with Surface-Enhanced Raman Scattering. In *2010 IEEE International Conference on Bioinformatics and Biomedicine (BIBM)*; 2010; pp 406−409. DOI: 10.1109/BIBM.2010.5706600.

(24) Alharbi, O.; Xu, Y.; Goodacre, R. *Analyst* **2014**, *139* (19), 4820−4827.

(25) Lussier, F.; Missirlis, D.; Spatz, J. P.; Masson, J.-F. *ACS Nano* **2019**, *13* (2), 1403−1411.

(26) Etchegoin, P. G.; Ru, E. C. L. *Phys. Chem. Chem. Phys.* **2008**, *10* (40), 6079−6089.

(27) Brulé, T.; Bouhelier, A.; Yockell-Lelièvre, H.; Clément, J.-E.; Leray, A.; Dereux, A.; Finot, E. *ACS Photonics* **2015**, *2* (9), 1266−1271.

(28) de Albuquerque, C. D. L.; Sobral-Filho, R. G.; Poppi, R. J.; Brolo, A. G. *Anal. Chem.* **2018**, *90* (2), 1248−1254.

(29) Premasiri, W. R.; Chen, Y.; Williamson, P. M.; Bandarage, D. C.; Pyles, C.; Ziegler, L. D. *Anal. Bioanal. Chem.* **2017**, *409* (11), 3043−3054.

(30) Wen-Yu Chiu, S.; Cheng, H.-W.; Chen, Z.-X.; Wang, H.-H.; Lai, M.-Y.; Wang, J.-K.; Wang, Y.-L. *Phys. Chem. Chem. Phys.* **2018**, *20* (12), 8032−8041.

(31) Handbook of Cyanobacterial Monitoring and Cyanotoxin Analysis https://www.wiley.com/en-us/Handbook+of+Cyanobacterial+Monitoring+and+Cyanotoxin+Analysis-p-9781119068686 (accessed Jun 25, 2019).

(32) Thrift, W. J.; Nguyen, C. Q.; Darvishzadeh-Varcheie, M.; Zare, S.; Sharac, N.; Sanderson, R. N.; Dupper, T. J.; Hochbaum, A. I.; Capolino, F.; Abdolhosseini Qomi, M. J.; et al. *ACS Nano* **2017**, *11* (11), 11317−11329.

(33) Pan, S. J.; Yang, Q. *IEEE Trans. Knowl. Data Eng.* **2010**, *22* (10), 1345−1359.

(34) Wang, P.; Pang, S.; Chen, J.; McLandsborough, L.; Nugen, S. R.; Fan, M.; He, L. *Analyst* **2016**, *141* (4), 1356−1362.

(35) Bodelón, G.; Montes-García, V.; Costas, C.; Pérez-Juste, I.; Pérez-Juste, J.; Pastoriza-Santos, I.; Liz-Marzán, L. M. *ACS Nano* **2017**, *11* (5), 4631−4640.

(36) Olson, A. P.; Ertsgaard, C. T.; Elliott, S. N.; Lindquist, N. C. *ACS Photonics* **2016**, *3* (3), 329−336.

(37) Lee, D. D.; Seung, H. S. *Nature* **1999**, *401* (6755), 788−791.

(38) Yampolsky, S.; Fishman, D. A.; Dey, S.; Hulkko, E.; Banik, M.; Potma, E. O.; Apkarian, V. A. *Nat. Photonics* **2014**, *8* (8), 650−656.

DOI: 10.1021/acs.analchem.9b03599
Anal. Chem. 2019, 91, 13337−13342

(39) Single Molecule SERS Spectral Blinking and Vibronic Coupling | *J. Phys. Chem. C* DOI: 10.1021/jp111345u (accessed Aug 16, **2019**).
(40) Etchegoin, P. G.; Le Ru, E. C. *Anal. Chem.* **2010**, *82* (7), 2888−2892.

DOI: 10.1021/acs.analchem.9b03599
Anal. Chem. 2019, 91, 13337−13342